




Rigid Registration of Point Clouds Based on Partial Optimal Transport

Hongxing Qin,¹  Yucheng Zhang,² Zhentao Liu³ and Baoquan Chen⁴

¹Chongqing University, Chongqing, China

²Baidu Online Network Technology, Beijing, China
apprenticeyc@163.com

³Chongqing University of Posts and Telecommunications, Chongqing, China
liuzhentao19961025@163.com

⁴Peking University, Beijing, China
baoquan@pku.edu.cn

Abstract

For rigid point cloud data registration, algorithms based on soft correspondences are more robust than the traditional ICP method and its variants. However, point clouds with severe outliers and missing data may lead to imprecise many-to-many correspondences and consequently inaccurate registration. In this study, we propose a point cloud registration algorithm based on partial optimal transport via a hard marginal constraint. The hard marginal constraint provides an explicit parameter to adjust the ratio of points that should be accurately matched, and helps avoid incorrect many-to-many correspondences. Experiments show that the proposed method achieves state-of-the-art registration results when dealing with point clouds with significant amount of outliers and missing points (see <https://www.acm.org/publications/class-2012>).

Keywords: point-based graphics, modelling, point-based methods, methods and applications

CCS Concepts: • Computing methodologies → Point-based models; Shape analysis

1. Introduction

Shape registration is a fundamental problem in computational geometry, computer vision, computer graphics and so on. With the developing of geometry scanning technology, point cloud registration is becoming an important step for 3D shape reconstruction from multiple scans. It aims to align two or more point clouds into a coherent coordinate frame by estimating their relative transformation.

Practical point set registration algorithms mainly include two components: assigning correspondences between two sets of points and computing the optimal transformation between two point sets in terms of the correspondences. Different point set registration algorithm have been proposed based on different correspondences. A constant number of random point correspondences are used in a variant of RANSAC algorithms [FB87, AMCO08, MAM14]. The fundamental limitation of RANSAC is that it does not generally provide the optimal solution because the optimal transformation is only on a constant number of random point correspondences. The assumption of iterative closest point (ICP) algorithm [BM92,

CSK05, GP02] is that the corresponding point of one source point is the nearest point in the target point cloud from the source point. Accurate correspondence heavily depends on the initial pose position of source and target point clouds. Therefore, ICP algorithm is susceptible to noise outliers and occlusions. Instead of one-to-one correspondence, one-to-many or many-to-many correspondences have been developed via a kernel function [TK04, MS10, JV10] to improve the robustness of registration algorithms on one-to-one correspondence. In general, registration algorithms based on fuzzy correspondence use the same kernel function to represent one-to-many correspondences. Thus, in these registration algorithm, two point clouds presumably represent the same shape model, and every point cloud is uniformly sampled from the shape model. Point cloud registration is still a challenging problem when the point clouds have many missing points or outliers.

In this study, we proposed a general framework for point cloud registration based on partial optimal transport [CPSV17]]. First, two point clouds are represented as two probability measures. The Wasserstein distance between two probability measures is

minimized to compute the transformation matrix between two point clouds. Compared with ICP methods, which use δ -function to represent the correspondence, and fuzzy correspondence methods, which uses the Gaussian function to represent the correspondence, the proposed method computes a more general transport plan to represent the correspondence. Furthermore, the mass conservation laws in traditional optimal transport are relaxed via a range constraint on the total mass to improve the robustness of point cloud registration algorithm when point clouds include a large part of outlier and missing points. The experiments demonstrate that the proposed approach elevates the robustness and accuracy of point cloud registration when point clouds include a large part of outlier and missing points. The source code can be found in <https://github.com/Hongxing-CQU/RPOT/>. Our contributions can be summarized as follows:

- We propose a point cloud registration algorithm based on optimal transport theory for partial overlap.
- The partial overlap problem is modelled by partial optimal transport via a hard marginal constraint.
- The hard marginal constraint provides an explicit parameter to adjust the ratio of points that should be accurately matched, and helps avoid incorrect soft correspondences.

2. Related Work

Rigid and non-rigid shape registration have been researched widely in past years. Our study belongs to rigid point cloud registration. Therefore, a brief survey has only been provided about the rigid point cloud registration methods. We also outlined the application of optimal transport in registration and state our contribution in this paper.

2.1. Rigid point cloud registration

Given two point clouds sets $P = \{x_i\}_{i \in I} \subset R^3$ and $Q = \{y_j\}_{j \in J} \subset R^3$, point cloud registration finds a transformation map F that makes the distance between two point clouds minimum. The distance between P and Q can generally be expressed as the weighted sum of point pair distance:

$$E = \sum_{i=1}^N \sum_{j=1}^M T(x_i, y_j) c(x_i, F(y_j)), \quad (1)$$

where $T(x_i, y_j)$ is the correspondence parameters, and $c(\cdot, \cdot)$ is the distance function between two points. Based on different point correspondences, the parameter $T(x_i, y_j)$ is set as a different function, and different point cloud registration methods are proposed.

RANSAC algorithm represents the minimization of the distance between two point clouds as a maximum consensus problem [FB87]. A constant number of random point correspondences are used in a variant of RANSAC algorithms [FB87, AMCO08, MAM14]. The weighted parameter is set as

$$T(x_i, y_j) = \begin{cases} 1 & (x_i, y_j) \in \mathcal{K}, \\ 0 & \text{others.} \end{cases}$$

where \mathcal{K} is the random point pairs. Aiger *et al.* [AMCO08] introduced 4-points congruent sets (4PCS) instead of triplets as a wide

basis in RANSAC. Mellado *et al.* [MAM14] improved the time complexity of 4PCS [AMCO08] from quadratic time to linear time via a smart indexing data organization. Gelfand *et al.* [GMGP05] proposed integral volume descriptor and developed a fast BnB algorithm based on distance matrix comparisons to select the optimal correspondence set. Álvaro Parra Bustos [APBC18] presented the guaranteed outlier removal approach to reduce the corresponding set. Zhou *et al.* [ZPK16] applied two stage of procedure to alleviate the effects of spurious correspondence. In the first step, reciprocity test and tuple test are applied to improve the inlier ratio of the correspondence set. Then, a robust objective function is optimized to provide a continuation of increasingly good approximation. RANSAC algorithms use the global search strategy to find the transformation map. However, the globally optimal solution cannot be obtained in general. The result of RANSAC algorithms is often used as the initialization to ICP method.

ICP [BM92], is the most important approach for rigid point cloud registration. The main reason is low computation cost and simplicity of ICP. In ICP, correspondences are set in terms of the closest distance criterion, which means

$$T(x_i, y_j) = \begin{cases} 1 & \text{if } d(x_i, y_j) < d(x_i, y_{j'}) (j \neq j', j' \in J), \\ 0 & \text{others.} \end{cases}$$

ICP is susceptible to local minima. Its performance critically relies on initialization quality and only local optimality is guaranteed. Different kinds of ICP algorithms have been developed to enhance the robustness of ICP algorithm. Chetverikov *et al.* [CSK05] applied the least trimmed squares approach to identify and reject outliers in Trimmed ICP. LM-ICP [Fit03] attempted to enlarge the basin of convergence by smoothing out the objective function to improve the robustness of ICP to poor initializations. They also directly used the Levenberg–Marquardt algorithm to minimize the registration error. Go-ICP [YLCJ15] presented a globally optimal algorithm by employing the conventional ICP algorithm with the branch-and-bound procedure. Sparse ICP [BTP13, MAP15] reformulated ICP algorithm using a sparse $l_p (p \leq 1)$ norm, instead of the classical squared l_2 norm, to learn the separation between data and outliers. However, these algorithms still depend on a good initial pose and orientation of point clouds.

Except for one-to-one correspondence, soft correspondence has also been used in point cloud registration. The correspondence between points is established via a probability function. The most commonly used probability function is Gaussian function, and the weighted parameter is set as

$$T(x_i, y_j) = \frac{\exp^{-\frac{1}{2} \left\| \frac{x_i - F(y_j)}{\sigma} \right\|^2}}{\sum_k \exp^{-\frac{1}{2} \left\| \frac{x_i - F(y_k)}{\sigma} \right\|^2}}. \quad (2)$$

Expectation maximization (EM)-ICP [GP02] algorithm formulates the rigid registration as a general maximum-likelihood estimation of the transformation and the matches. In Haile and Anand [HA03], the transformation map and correspondence parameters are optimized jointly for point cloud registration. Coherent point drift (CPD) [MS10] considers the alignment of two point sets a probability density estimation problem and fits the Gaussian mixture model centroids to the data by maximizing the likelihood. These methods use EM algorithm to optimize correspondence parameters and

transformation map iteratively. Jian and Vemuri [JV10] first represented two point sets as two distribution. Then, the point set registration problem is reformulated as the alignment of two distributions. Gao and Tedrake [GT19] proposed FilerReg by formulating the E-step as a Gaussian filtering problem to improve the computational performance of probabilistic registration method. Eckart et al. [EKK18] proposed hierarchical Gaussian mixture for adaptive 3D registration. The methods based on probability correspondence performs better than ICP algorithms for point cloud registration in the presence of noise, outliers and missing points. The probability correspondence of point cloud registration is based on the point distribution as a whole. When two point sets have severe outliers or missing points, the point sets can be sampled from different shape, and the methods on the probability correspondence do not provide an efficient strategy to eliminate the effects of outliers or missing points locally. With the aim to address this problem, our approach provides more general correspondence parameters than the probability correspondence, and achieves state-of-the-art performance. Recently, the methods on deep learning, such as DeepICP [LWZ*19] and deep closest point (DCP) [WS19] have also been developed. The correspondence parameter is obtained via the *Softmax* function. Compared with the methods on deep learning, the correspondence parameter in our approach is only learned from the point clouds, which need to be registered.

2.2. Optimal transport and registration on optimal transport

Optimal transport is becoming an import approach in computer graphics [QCHC17, QHL*19, SDGP*15, BC19], computer vision [RTG00] and machine learning [FMS19]. Optimal transport theory is roughly reviewed in this section. More details can be found in Villani[Vil08]. Given a space Ω , the distance metric on the space is represented as $c : \Omega \times \Omega \rightarrow \mathbb{R}_+$. $P(\Omega)$ and $P(\Omega \times \Omega)$ are used to represent the sets of probability measure on the space Ω and the product space $\Omega \times \Omega$. For a probability measure $\mu \in P(\Omega)$, it satisfies

$$\mu(\emptyset) = 0, \mu(\Omega) = 1, 0 \leq \mu(U) \leq 1(U \subseteq \Omega).$$

The optimal transport problem is about the optimal transport plan and the minimum cost between two probability measures $\mu \in P(\Omega)$ and $\nu \in P(\Omega)$. It is formulized as:

$$\inf_{\pi \in \Pi(\mu, \nu)} \int_{\Omega \times \Omega} c(x, y) d\pi, \quad (3)$$

where $c(x, y)$ is the cost function, and $\pi \in P(\Omega \times \Omega)$ is the transport plan. For balance optimal transport problem, transport plan meets the constrain:

$$\pi(\cdot, \Omega) = \mu, \pi(\Omega, \cdot) = \nu \quad (4)$$

where $\pi(\cdot, \Omega)$ and $\pi(\Omega, \cdot)$ are separately two marginal measures.

A fundamental property of classical optimal transport is that it requires the transport plan to meet the mass conservation laws (Equation 4). However, some applications, such as registration of point clouds with outliers and missing points, may require optimal

transport algorithms to handle the unbalanced optimal problem, in which the mass conservation law is broken.

In Chizat et al. [CPSV16], Unbalanced optimal transport problems has been modelled as:

$$\min_{\pi \in P(\Omega \times \Omega)} \int_{\Omega \times \Omega} c(x, y) d\pi + D_1(\pi(\cdot, \Omega) | \mu) + D_2(\pi(\Omega, \cdot) | \nu), \quad (5)$$

where $D_i(\cdot | \cdot)$ is a divergence function and provides a sense of how close two measures are. For a traditional optimal transport problem, the divergence function is the equality constraint:

$$t_{\{=\}}(\mu | \nu) = \begin{cases} 0 & \mu = \nu, \\ \infty & \text{others.} \end{cases}$$

When another divergence function is selected as the divergence function, such as the KL divergence or the total variation distance, mass conservation law is broken. Equation (5) represents an unbalanced optimal transport problem.

As a similarity measure, Wasserstein distance, is also applied for shape registration [HZTA04, SNB*12, SWS*15, FCVP17, RH17, BC19]. Hanker et al. [HZTA04] found the registration mapping between images by minimizing the L^2 Kantorovich-Wasserstein distance under a mass preservation. Solomon et al. [SNB*12] applied optimal transport theory to the problem of mapping between two nonisometric surfaces. Feydy et al. [FCVP17, FRTG19] introduced the unbalanced optimal transport methods for diffeomorphic matching of imaging data via KL divergence. In the paper, Feydy et al.'s approach [FCVP17] is labelled as KL. Although the mass preservation law is broken by using KL divergence. in Feydy et al. [FCVP17], the proposed algorithm cannot be efficiently applied to the registration of point clouds with severe outliers or missing points. The main reason is that the transport plan, obtained on an accurate registration, may lead to a high KL divergence when point clouds have severe outliers or missing points. Therefore, the optimal transport plan obtained from Feydy et al. [FCVP17] cannot describe the accurate correspondence between two point clouds with severe outliers or missing points (Figure 1). In sliced partial optimal transport (SPOT), Bonneel and Coeurjolly [BC19] proposed a one-dimensional partial transport solver and extended ICP algorithm using optimal transport. However, SPOT is based on the assumption that all points from the source distributions need to be matched to (part of) the target distribution. When the part of the source points cannot be matched with the points of the target points, an accurate registration cannot be obtained in SPOT.

3. Method

An accurate estimation of correspondences is the key to align two point sets P and Q in arbitrary initial positions (Figure 1). When two point sets have severe outliers or missing points, some points in one point set cannot be matched with any point in another point set. The algorithms CPD [MS10] and KL [FCVP17] on soft correspondence are based on global correspondences as a whole. In CPD algorithm [MS10], the weighted differences between all combinations of points have been considered. In KL approach [FCVP17], the missing mass of every point will be considered in the cost function, and the mass of every point from different point sets is

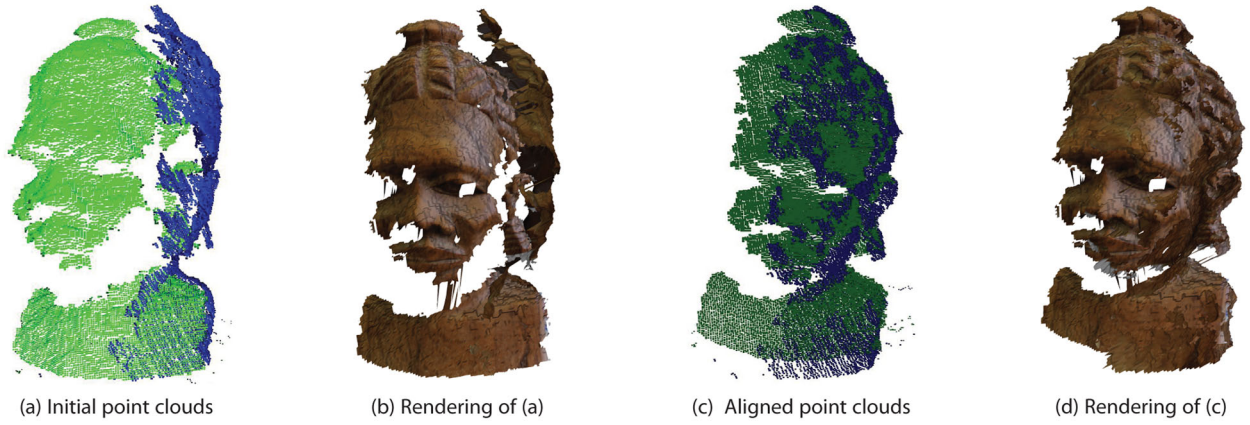


Figure 1: Comparison among different methods on correspondences when point clouds to be registered have severe missing points.

different if there are different number of points in two point sets. To decrease the weighted difference in CPD algorithm [MS10] and make a balance between the missing mass cost and the transport cost in Feydy *et al.* [FCVP17], the optimal registration result cannot be obtained with the algorithms CPD [MS10] and KL [FCVP17] in Figure 1. In this study, we view the registration of point clouds as a partial optimal transport problem to improve the robustness of the previous algorithms for point clouds with severe outliers or missing points by explicitly eliminating the wrong correspondence induced by severe outliers or missing points.

3.1. Modelling on partial optimal transport

The procedure of point set registration includes two steps: assigning correspondence and computing transformation map. In this section, assigning correspondences and recovering the transformation are modelled as a unified optimization problem.

Given two point clouds sets $P = \{x_i\}_{i \in I} \subset R^3$ and $Q = \{y_j\}_{j \in J} \subset R^3$, two discrete probability measures in R^3 are defined as

$$\mu = \sum_{i=1}^m \rho_i \delta_{x_i}, \text{ s.t. } \sum_{i=1}^m \rho_i = 1, \rho_i \geq 0, \delta_{x_i} = \begin{cases} 1 & x_i \in P, \\ 0 & \text{others,} \end{cases} \quad (6)$$

and

$$\nu = \sum_{j=1}^n \phi_j \delta_{y_j}, \text{ s.t. } \sum_{j=1}^n \phi_j = 1, \phi_j \geq 0, \delta_{y_j} = \begin{cases} 1 & y_j \in Q, \\ 0 & \text{others,} \end{cases} \quad (7)$$

where m and n are the number of points in P and Q , respectively. Then, we model the registration of P and Q as a partial optimal transport problem, that is

$$\begin{aligned} & \arg \min_{\mathbf{R}, \mathbf{t}, \pi} \sum_{i=1}^m \sum_{j=1}^n c(x_i, F(y_j)) \pi(x_i, y_j) \\ & + D_1(\pi \mathbf{1}_n | \mu) + D_2(\pi^T \mathbf{1}_m | \nu) + D_3\left(\sum_{i=1}^m \sum_{j=1}^n \pi(x_i, y_j) | 1\right), \end{aligned} \quad (8)$$

The transformation function F includes the rotation transformation \mathbf{R} and the translation transformation \mathbf{t} . The transport plan π presents

the correspondence between P and Q . The first term measures the cost of transporting the mass from μ to ν in terms of transport plan π . The first term is the same as the distance between the two point clouds defined in Equation (1). In the second and third terms,

$$\pi \mathbf{1}_n = \left(\sum_{j=1}^n \pi(x_1, y_j) \quad \sum_{j=1}^n \pi(x_2, y_j) \quad \cdots \quad \sum_{j=1}^n \pi(x_m, y_j) \right)^T$$

and

$$\pi^T \mathbf{1}_m = \left(\sum_{i=1}^m \pi(x_i, y_1) \quad \sum_{i=1}^m \pi(x_i, y_2) \quad \cdots \quad \sum_{i=1}^m \pi(x_i, y_n) \right)^T.$$

The divergences $D_1(\cdot | \cdot)$ and $D_2(\cdot | \cdot)$ are two constraints on the marginals of π , which maintain that the marginals of π are close to the probability measures μ and ν , separately. In our work, the divergences $D_1(\cdot | \cdot)$ and $D_2(\cdot | \cdot)$ are represented as a range constraint:

$$RG_{[\alpha_1, \beta_1]}(\pi \mathbf{1}_n | \mu) = \begin{cases} 0 & \alpha_1 \mu \leq \pi \mathbf{1}_n \leq \beta_1 \mu \\ +\infty & \text{others,} \end{cases} \quad (9)$$

and

$$RG_{[\alpha_1, \beta_1]}(\pi^T \mathbf{1}_m | \nu) = \begin{cases} 0 & \alpha_1 \nu \leq \pi^T \mathbf{1}_m \leq \beta_1 \nu \\ +\infty & \text{others.} \end{cases} \quad (10)$$

Equations (9) and (10) represent that the transported mass between points x_i and y_j is constrained in terms of the range of $[\alpha_1, \beta_1]$. The proposed method is labelled as RG. Compared with traditional optimal transport, the range constraint divergence (Equations 9 and 10) relaxes the mass transport, and breaks the mass conservation law. In our work, α_1 and β_1 are set to 0 and 1, respectively, for D_1 and D_2 . $\alpha_1 = 0$ makes 0-transportation possible when $x_i \in P$ or $y_j \in Q$ does not have any correspondence in Q or P . 0-transportation means $\sum_{j=1}^n \pi(x_i, y_j) = 0$. $\beta_1 = 1$ means that the mass transported from x_i cannot be more than ρ_i . Therefore, the second and third terms are constraint terms for the mass transformed from x_i and the mass transformed to y_j . Compared with D_1 and D_2 , the fourth term is a constraint term on the total mass. We also use the range constraint divergence $RG_{[\alpha_2, \beta_2]}$ for D_3 , and set $\alpha_2 = 0$ and $\beta_2 \in (0, 1]$. For D_3 , β_2 is a free parameter to control the mass, which can be transformed. It can be transformed between point clouds in term of the overlap of the two shape. When the point cloud P in Figure 2 has severe miss-

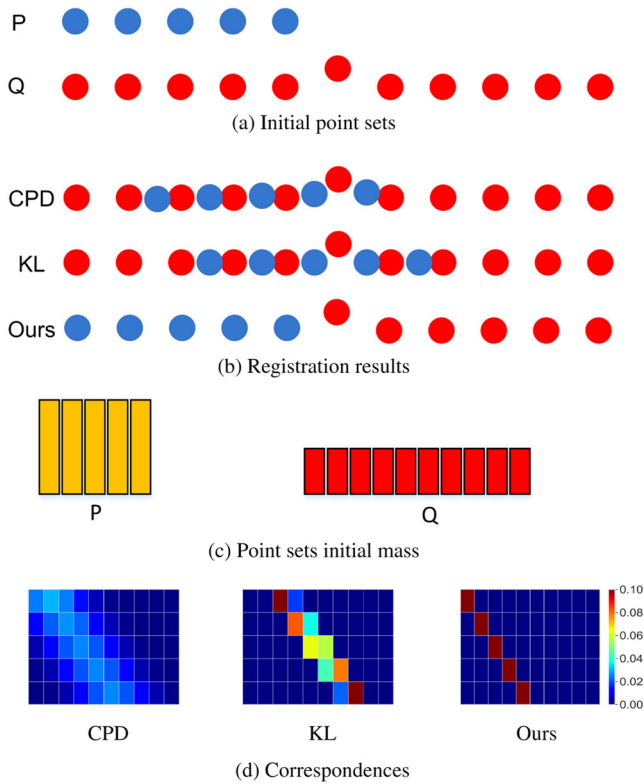


Figure 2: Registration results in different β_2 and λ values.

Algorithm 1. Rigid point clouds registration on partial mass optimal transport

Data: Point clouds \mathbf{P} and \mathbf{Q} , initial entropy parameter ϵ , ϵ -scaling parameter λ , threshold parameter η

Result: Rotation matrix \mathbf{R} , Translation vector \mathbf{t}

Initiation: $\mathbf{R}_0 = \mathbf{R}_1 = \mathbf{I}$, $\mathbf{t} = \mathbf{0}$, $\rho_i = \frac{1}{m}$ ($i = 1, \dots, m$),

$\phi_j = \frac{1}{n}$ ($j = 1, \dots, n$), the threshold η , the iterating vector

$\mathbf{b} = \mathbf{1}_m$, $Iter = true$;

Compute the barycenters B_p and B_q of P and Q ;

$\mathbf{X} = \mathbf{P} \ominus B_p$;

$\mathbf{Y} = \mathbf{Q} \ominus B_q$ (\ominus is an entrywise minus operator);

repeat

$\mathbf{R}_0 = \mathbf{R}_1$;

 Assign correspondence π (Algorithm 2);

 Recover transformation \mathbf{R}_1 and \mathbf{t} (Algorithm 3);

$\epsilon = \epsilon\lambda$;

until $\|\mathbf{R}_1 - \mathbf{R}_0\|_F < \eta$;

return \mathbf{R}_1 , \mathbf{t} ;

ing points, only a part of Q can be matched with P . In this case, a perfect registration result can be obtained when β_2 is set as a value close to the overlap of two point clouds.

We apply a loop iteration algorithm (Algorithm 1) to recover the transformation $F(\cdot)$. The transport plan π and the transformation

$F(\cdot)$ are computed by minimizing the variational problem (Equation 8) step by step.

3.2. Assignment of correspondences

From the first term in Equation (8), the transport plan π represents the correspondences between P and Q . We first fix the transformation (\mathbf{R}, \mathbf{t}) in the minimization step over the transport plan. Then, the optimal transport problem (Equation 8) is approximated via an entropy term $H(\cdot)$, that is,

$$\arg \min_{\pi} \sum_{i=1}^m \sum_{j=1}^n c(x_i, F(y_j)) \pi(x_i, y_j) + \epsilon H(\pi) \quad (11)$$

$$+ D_1(\pi \mathbf{1}_n | \mu) + D_2(\pi^T \mathbf{1}_m | \nu) + D_3(\mathbf{1}_m^T \pi \mathbf{1}_n | 1),$$

where $H(\pi)$ is the entropy of π

$$H(\pi) = \sum_{i=1}^m \sum_{j=1}^n \pi(x_i, y_j) (\log \pi(x_i, y_j) - 1),$$

and ϵ is a positive regularization parameter, which controls the degree of regularization. Equation (11) is a convex optimization problem. The first half of Equation (11) is the optimal mass transport problem with the entropy regularization term [SDGP*15]. Thus, Equation (11) can be represented as

$$\arg \min_{\pi} D_1(\pi \mathbf{1}_n | \mu) + D_2(\pi^T \mathbf{1}_m | \nu) + D_3(\mathbf{1}_m^T \pi \mathbf{1}_n | 1) + \epsilon KL(\pi | K), \quad (12)$$

where $K_{ij} = e^{-\frac{c(x_i, y_j)}{\epsilon}}$, and $KL(\cdot | \cdot)$ is the KL divergence function. Following [CPSV16], the optimal transport plan can be represented as

$$\pi = \exp(z/\epsilon) \text{diag}(\exp(\mathbf{u}/\epsilon)) \mathbf{K} \text{diag}(\exp(\mathbf{v}/\epsilon)) \quad (13)$$

where \mathbf{u} , \mathbf{v} and z are the solution of the dual problem of Equation (11). The dual problem is

$$\arg \max_{(\mathbf{u}, \mathbf{v}, z) \in (\mathbb{R}^m, \mathbb{R}^n, \mathbb{R})} -D_1^*(-\mathbf{u}) - D_2^*(-\mathbf{v}) - D_3^*(-z) - \epsilon KL^*(\mathbf{u} \mathbf{1}_n^T + \mathbf{v} \mathbf{1}_m^T + z \mathbf{1}_m^T \mathbf{1}_n | K), \quad (14)$$

where the function $*(\cdot)$ is the convex conjugate of the function $\cdot(\cdot)$.

The dual problem (Equation 14) can be solved by alternating optimization in \mathbf{u} , \mathbf{v} and z . When (\mathbf{v}, z) , (\mathbf{u}, z) and (\mathbf{u}, \mathbf{v}) are fixed separately, the corresponding maximization functions are obtained as

$$\max_{\mathbf{u}} -D_1^*(-\mathbf{u}) - \epsilon KL^*(\mathbf{u}/\epsilon | \exp(z/\epsilon) \mathbf{K} \exp(\mathbf{v}/\epsilon)),$$

$$\max_{\mathbf{v}} -D_2^*(-\mathbf{v}) - \epsilon KL^*(\mathbf{v}/\epsilon | \exp(z/\epsilon) \mathbf{K}^T \exp(\mathbf{u}/\epsilon)), \quad (15)$$

$$\max_z -D_3^*(-z) - \epsilon KL^*(z/\epsilon | \exp(\mathbf{u}^T/\epsilon) \mathbf{K} \exp(\mathbf{v}/\epsilon)).$$

Furthermore, the new variables \mathbf{a} , \mathbf{b} and g are introduced:

$$\mathbf{a} = \exp(\mathbf{u}/\epsilon) \quad \mathbf{b} = \exp(\mathbf{v}/\epsilon) \quad g = \exp(z/\epsilon). \quad (16)$$

Algorithm 2. Assigning correspondence

Data: Point clouds \mathbf{X} , transformed point clouds \mathbf{Y} , two probability measures μ and ν , initial entropy parameter ϵ , transport plan π , iterating vector \mathbf{b} , the parameter β_2 of range constraint term D_3 , iterating parameter g

Result: transport plan π and iterating vector \mathbf{b}
Compute distance matrix \mathbf{c} and the kernel matrix \mathbf{K} ;

repeat

$$\begin{aligned} \mathbf{a} &\leftarrow \min(\beta_1 \mu, \max(\alpha_1 \mu, g \mathbf{K} \mathbf{b})) \oslash g \mathbf{K} \mathbf{b}; \\ \mathbf{b} &\leftarrow \min(\beta_1 \nu, \max(\alpha_1 \nu, g \mathbf{K}^T \mathbf{a})) \oslash g \mathbf{K}^T \mathbf{a}; \\ g &\leftarrow \min(\beta_2, \max(\alpha_2, \mathbf{a}^T \mathbf{K} \mathbf{b})) \oslash \mathbf{a}^T \mathbf{K} \mathbf{b}; \end{aligned}$$

until until \mathbf{b} is convergence;

$\pi \leftarrow g \text{diag}(\mathbf{a}) \mathbf{K} \text{diag}(\mathbf{b})$;

return π, \mathbf{b} ;

The alternating optimization, via dual theory, then becomes:

$$\begin{aligned} \mathbf{a}^{l+1} &= \text{prox}_{D/\epsilon}^{KL}(g \mathbf{K} \mathbf{b}^l) \oslash g \mathbf{K} \mathbf{b}^l, \\ \mathbf{b}^{l+1} &= \text{prox}_{D/\epsilon}(g \mathbf{K}^T \mathbf{a}^{l+1}) \oslash g \mathbf{K}^T \mathbf{a}^{l+1}, \\ g^{l+1} &= \text{prox}_{D/\epsilon}^{KL}((\mathbf{a}^{l+1})^T \mathbf{K} \mathbf{b}^{l+1}) \oslash (\mathbf{a}^{l+1})^T \mathbf{K} \mathbf{b}^{l+1}, \end{aligned} \quad (17)$$

where \oslash denotes entrywise division, and $\text{prox}_{D/\epsilon}^{KL}(\cdot)$ is a proximal operator, and is defined as

$$\text{prox}_{D/\epsilon}^{KL}(\mathbf{w}) = \arg \min_{\mathbf{s} \in R^n} D(\mathbf{s}) + \epsilon KL(\mathbf{s} | \mathbf{w}). \quad (18)$$

When $RG_{[\alpha, \beta]}(\cdot | \mathbf{w})$ is selected as $D(\cdot)$ in our work, the output of the operator $\text{prox}_{D/\epsilon}^{KL}(\mathbf{w})$ is

$$\text{prox}_{D/\epsilon}^{KL}(\mathbf{w}) \rightarrow \min(\beta \mathbf{w}, \max\{\alpha \mathbf{w}, \mathbf{s}\}).$$

Then, the transport plan can be obtained as

$$\pi = g \cdot \text{diag}(\mathbf{a}) \mathbf{K} \text{diag}(\mathbf{b}).$$

Algorithm 2 describes the pseudocode of the minimization step over the transport plan π .

3.3. Recovering transformation

Point clouds \mathbf{P} and \mathbf{Q} are represented as $\mathbf{P} = (\mathbf{x}_1 \mathbf{x}_2 \dots \mathbf{x}_m)^T$ and $\mathbf{Q} = (\mathbf{y}_1 \mathbf{y}_2 \dots \mathbf{y}_n)^T$. Make \mathbf{P} and \mathbf{Q} close enough is necessary to efficiently align the point clouds \mathbf{P} and \mathbf{Q} . Therefore, we first translate \mathbf{P} and \mathbf{Q} to make them with same barycenter as a preprocessing step, that is,

$$\mathbf{X} = \mathbf{P} \ominus \mathbf{B}_p, \quad \mathbf{Y} = \mathbf{Q} \ominus \mathbf{B}_q,$$

where \ominus is an entrywise minus operator, \mathbf{B}_p and \mathbf{B}_q are the barycenters of \mathbf{P} and \mathbf{Q} :

$$\mathbf{B}_p = \sum_{i=1}^m \rho_i \mathbf{x}_i, \quad \mathbf{B}_q = \sum_{j=1}^n \varrho_j \mathbf{y}_j.$$

In Equation (8), the transformation map F only depends on the first term. For rigid transformation, the transformation map is rep-

resented as $F(\mathbf{y}_j) = \mathbf{R} \mathbf{y}_j - \mathbf{t}$, where \mathbf{R} and \mathbf{t} are the rotation matrix and translation vector. Recovering transformation, therefore, is represented as the minimization problem:

$$\arg \min_{\mathbf{R}, \mathbf{t}} E, \quad E = \sum_{i=1}^m \sum_{j=1}^n \pi(\mathbf{x}_i, \mathbf{y}_j) \|\mathbf{x}_i - \mathbf{R} \mathbf{y}_j - \mathbf{t}\|^2. \quad (19)$$

Let $\nabla E_i = 0$. We can obtain the close form expression for \mathbf{t} as follows:

$$\mathbf{t} = \mathbf{u}_x - \mathbf{R} \mathbf{u}_y, \quad (20)$$

where

$$\mathbf{u}_x = \frac{\mathbf{X}^T \pi \mathbf{1}_n}{\sum_{i,j=1}^{m,n} \pi_{i,j}}, \quad \mathbf{u}_y = \frac{\mathbf{Y}^T \pi^T \mathbf{1}_m}{\sum_{i,j=1}^{m,n} \pi_{i,j}}. \quad (21)$$

The energy function E is rewritten as follows by replacing translation \mathbf{t} in the objective function E :

$$E = \sum_{i=1}^M \sum_{j=1}^N \pi_{ij} \|(\mathbf{x}_i - \mathbf{u}_x) - \mathbf{R}(\mathbf{y}_j - \mathbf{u}_y)\|^2. \quad (22)$$

We define

$$\hat{\mathbf{x}}_i = \mathbf{x}_i - \mathbf{u}_x, \quad \hat{\mathbf{y}}_j = \mathbf{y}_j - \mathbf{u}_y. \quad (23)$$

The following is obtained by substituting $\hat{\mathbf{x}}_i$ and $\hat{\mathbf{y}}_j$ into Equation (22) and omitting the constant term:

$$E = - \sum_{i=1}^M \sum_{j=1}^N \pi_{ij} \hat{\mathbf{x}}_i^T \mathbf{R} \hat{\mathbf{y}}_j = - \text{tr}(\pi^T \hat{\mathbf{X}} \mathbf{R} \hat{\mathbf{Y}}).$$

The minimization of E is obtained by the maximization of the trace. We obtain the following by using the trace property $\text{tr}(\mathbf{A} \mathbf{B}) = \text{tr}(\mathbf{B} \mathbf{A})$: we obtain

$$\text{tr}(\pi^T \hat{\mathbf{X}} \mathbf{R} \hat{\mathbf{Y}}^T) = \text{tr}(\mathbf{R} \hat{\mathbf{Y}}^T \pi^T \hat{\mathbf{X}}).$$

The matrix $\hat{\mathbf{Y}}^T \pi^T \hat{\mathbf{X}}$ is represented as $\mathbf{U} \mathbf{A} \mathbf{V}^T$ via singular value decomposition. We obtain the following by using the trace property again:

$$\text{tr}(\mathbf{R} \hat{\mathbf{Y}}^T \pi^T \hat{\mathbf{X}}) = \text{tr}(\mathbf{R} \mathbf{U} \mathbf{A} \mathbf{V}^T) = \text{tr}(\mathbf{A} \mathbf{V}^T \mathbf{R} \mathbf{U}). \quad (24)$$

Let $\mathbf{W} = \mathbf{V}^T \mathbf{R} \mathbf{U}$. The matrixes \mathbf{V}^T , \mathbf{R} and \mathbf{U} are all orthogonal matrix. Thus, \mathbf{W} is also an orthogonal matrix. For every column vector \mathbf{W}_j in \mathbf{W} , the property $\mathbf{W}_j^T \mathbf{W}_j = 1$ exists. Therefore, all entries W_{ij} are not larger than 1. Given that \mathbf{A} is a diagonal matrix with $A_{ii} \geq 0$, the trace $\text{tr}(\mathbf{A} \mathbf{V}^T \mathbf{R} \mathbf{U})$ is maximized if $W_{ii} = 1$. Then, we obtain the equation

$$\mathbf{I} = \mathbf{W} = \mathbf{V}^T \mathbf{R} \mathbf{U}$$

and derivate the rotation matrix:

$$\mathbf{R} = \mathbf{V} \mathbf{C} \mathbf{U}^T, \quad \mathbf{C} = \text{diag}(1, \dots, \det(\mathbf{V} \mathbf{U}^T)). \quad (25)$$

Algorithm 3 describes the pseudocode of the step of recovering transformation.

Algorithm 3. Recovering transformation

Data: Point clouds \mathbf{X} and \mathbf{Y} , correspondences π
Result: Rotation matrix \mathbf{R} , Translation vector \mathbf{t}
 Compute \mathbf{u}_x and \mathbf{u}_y (Eq. 21);
 Compute $\widehat{\mathbf{X}}$ and $\widehat{\mathbf{Y}}$ (Eq. 23);
 Compute SVD \mathbf{UAV}^T of $\widehat{\mathbf{X}}^T \pi^T \widehat{\mathbf{X}}$;
 Compute rotation matrix \mathbf{R} (Eq. 25);
 Compute translation vector \mathbf{t} (Eq. 20);
return \mathbf{R} and \mathbf{t}

Table 1: Parameters.

Fig.	1	7	8	9.a	9.b	10	11	12	13	14.a	14.b	14.c	15	16	17
β_2	0.6	1	1	1	1	0.55	0.55	0.55	0.6	0.6	1	1	0.9	0.8	0.9
λ	0.95	0.9	0.8	0.99	0.7	0.995	0.995	0.9	0.9	0.9	0.9	0.9	0.95	0.95	0.95

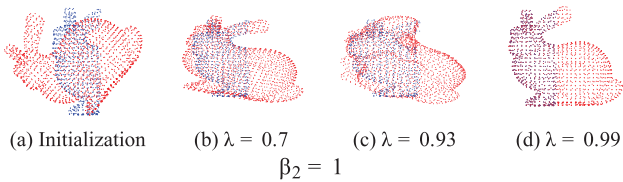


Figure 3: Registration results in different λ values.

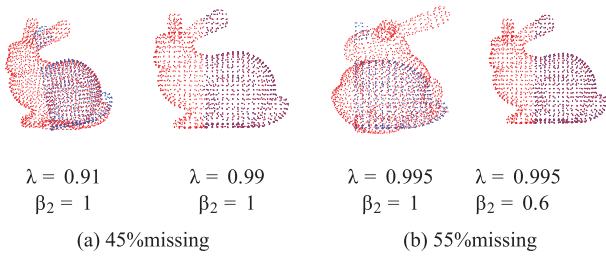


Figure 4: Comparison of running time between RG and KL.

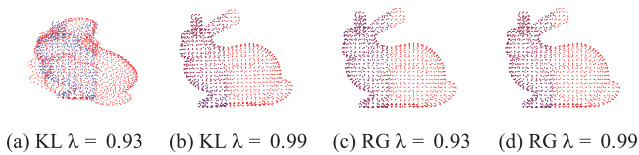
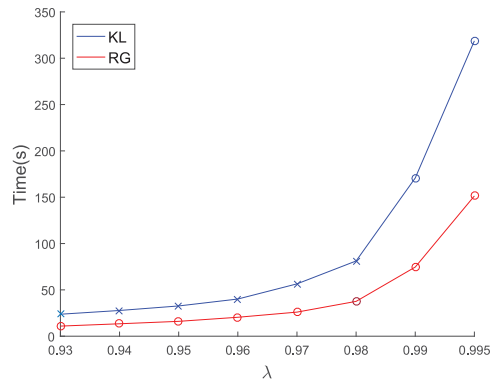


Figure 5: Comparison between KL and RG methods. We set $\beta_2 = 0.6$ for KG.

Table 2: Comparison between KL and RG methods in different values of β_2 and λ .

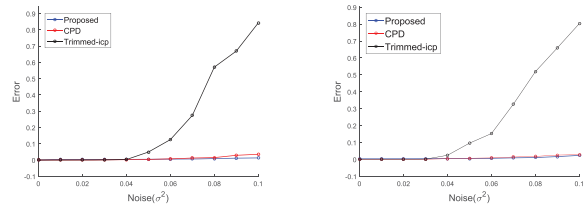
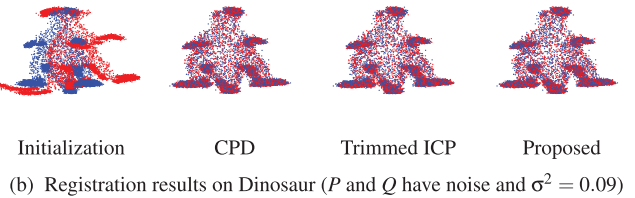
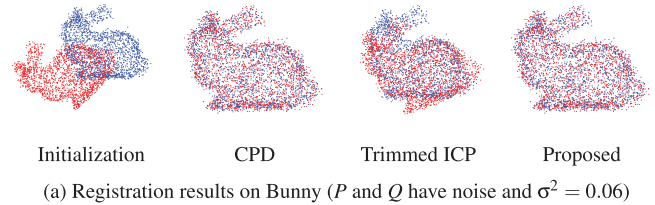
λ	0.93	0.94	0.95	0.96	0.97	0.98	0.99
$RG_{[0,1]}$	×	×	×	×	×	×	✓
KL	×	×	×	×	×	×	✓
$RG_{[0,0.6]}$	✓	✓	✓	✓	✓	✓	✓

× means angular error is larger than 1. ✓ means angular error is no more than 0.1.

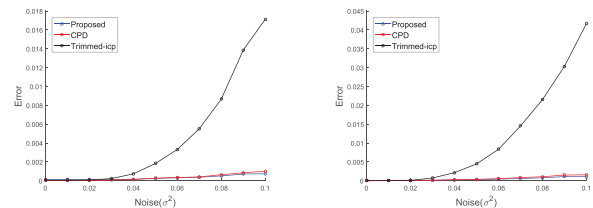


(a) Time comparison

Figure 6: The proposed algorithm is applied to two point clouds with only 30% overlap.

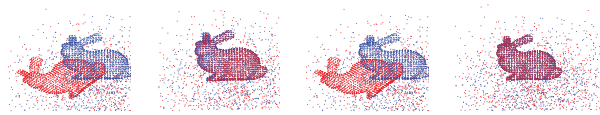


(c) Error curves on Bunny model with different levels of noise.

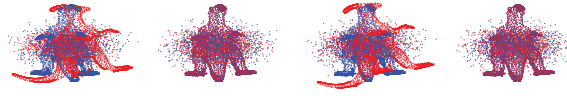


(d) The error curve on Dinosaur model with different level of noise.

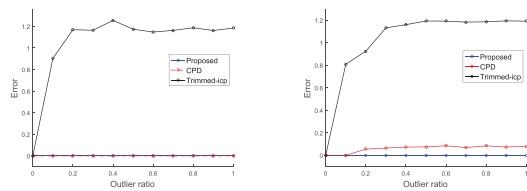
Figure 7: Comparison of point clouds with different levels of noise.



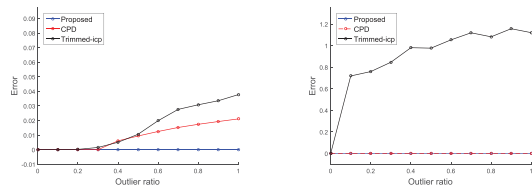
(a) Registration results on Bunny (P and Q have the same outlier ratio of 0.6).



(b) Registration results on Dinosaur (P and Q have the same outlier ratio of 0.5).



(c) Error curves on Bunny model with different levels of outlier.

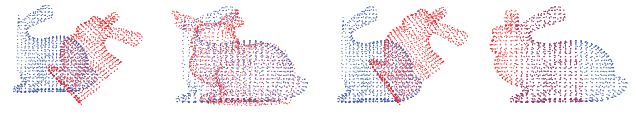


(d) Error curves on Dinosaur model with different levels of outlier.

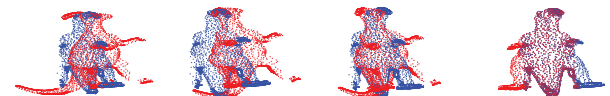
Figure 8: Comparison of point clouds with different levels of outliers.

4. Experiment

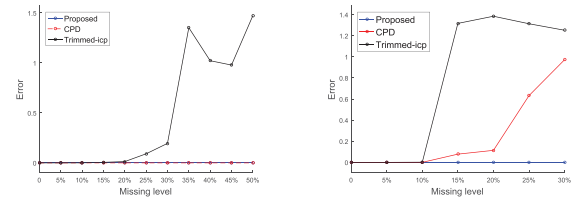
We run our algorithm on real scanned point clouds and synthetic point clouds with severe noise, outliers and missing parts, to test the robustness and accuracy of the proposed algorithm. We also make comparison on experiment results between our approach and state-of-the-art methods. In our experiments, we set ρ_i and ϕ_j as $1/m$ and $1/n$. If no special declaration exists, the parameters of range constraint term are set as $\eta = 1e-5$, $\alpha_1 = \alpha_2 = 0$ and $\beta_1 = \beta_2 = 1$. The parameters in experiments are listed in Table 1. We also introduce the outliers ratio and the missing ratio to represent the level of outliers and missing points. The outliers ratio is defined as the ratio of the number of added outliers and the number of original point clouds. The missing ratio is the ratio of the number of missing points and the number of original points. We use the angular and translation error of the estimated relative transformation (\mathbf{R}, \mathbf{T}) against the ground truth ($\bar{\mathbf{R}}, \bar{\mathbf{T}}$) to evaluate the performance. The angular error is calculated as $2\sin^{-1}(\frac{\|\mathbf{R}-\bar{\mathbf{R}}\|_F}{\sqrt{8}})$, where $\|\mathbf{R}-\bar{\mathbf{R}}\|_F$ is



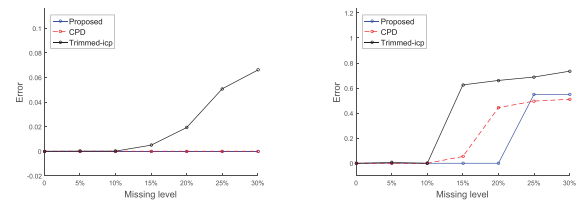
(a) Registration results on Bunny (P and Q have missing points. The missing ratio is 25%).



(b) Registration results on Dinosaur (P and Q have missing points. The missing ratio is 20%).



(c) Error curves on Bunny model with different levels of missing points.



(d) Error curves on Dinosaur model with different levels of missing points.

Figure 9: Comparison of point clouds with different levels of missing points.

Frobenius norm of the rotation matrix. The translation error is calculated as $\|\mathbf{T} - \bar{\mathbf{T}}\|_2$.

4.1. Effect of parameters

Parameters ϵ and β_2 are free parameters. Parameter ϵ plays the role of controlling the scale of $\pi(\cdot, \cdot)$. The larger the ϵ is, the higher the scale of $\pi(\cdot, \cdot)$ is, and the mass of every point is transformed to more farther points. Conversely, the smaller ϵ is, the more mass of every point x_i is transformed to the closer points y_j from x_i . Thus, the larger the ϵ , more global structure of point cloud is considered during the registration procedure. The smaller the ϵ is, more local structure of point cloud is considered during the registration procedure. In this

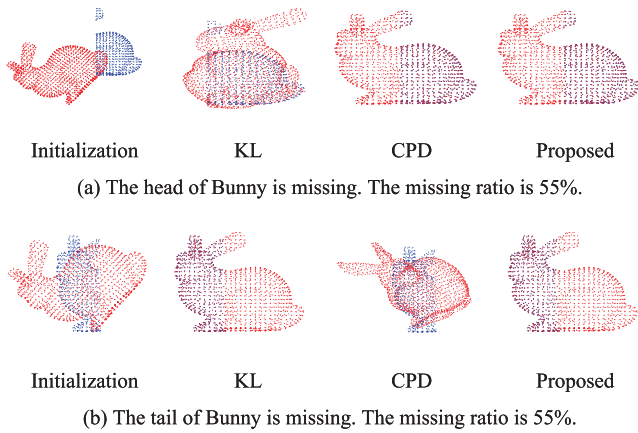


Figure 10: Comparisons of point clouds with severe missing points among KL, CPD and RG.

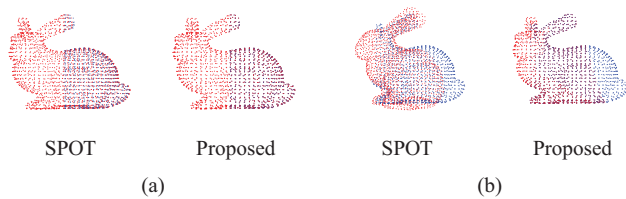


Figure 11: Comparisons between SPOT and the proposed method. In (a), the source point set has missing points, and the missing ratio is 50%. In (b), both the source point sets and the target source point set have missing points, and the missing ratio is 20%.

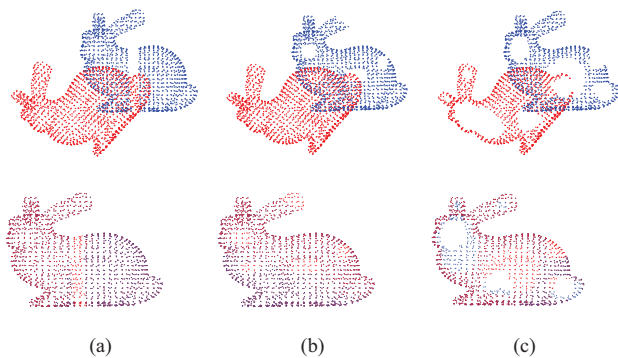


Figure 12: Registration on point clouds with different missing points. The missing ratios are 20%, 20% and 50% in (a), (b) and (c) separately.

study, we apply an iterated procedure to update ϵ step by step via an ϵ -scaling parameter λ , that is

$$\epsilon = \lambda \epsilon \quad (0 < \lambda < 1).$$

On the one hand, a larger ϵ considers more global structures and reduces the influence of noise and missing points in the early stage of the registration procedure. On the other hand, a smaller ϵ considers

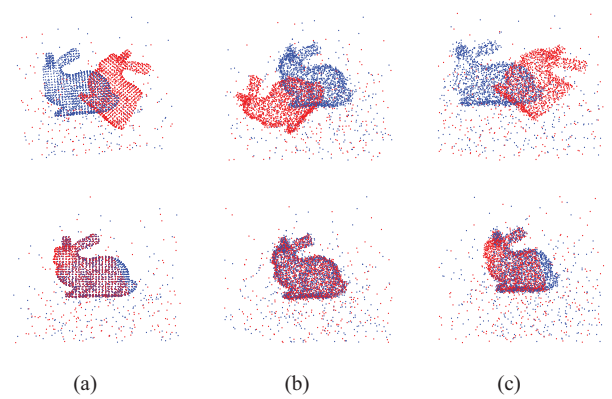


Figure 13: Registration on point clouds corrupted by different combinations of noise, outliers and missing points. In (a), point clouds are corrupted by outliers and missing points. In (b), point clouds are corrupted by outliers and noise. In (c), point clouds are corrupted by outliers, noise and missing points.

more local structure and provides an accurate transformation matrix at the end stage of the registration procedure.

In our experiments, the initial value of ϵ is set as 0.004. λ controls the descent speed of ϵ , and makes local structures be considered mainly at the early stage of iteration. When point clouds are with severe missing points or noise, it is easy to fall into a local optimum (Figure 3) if a small λ is used. When a large λ is used global structures and local structures can be considered simultaneously during the registration procedure, and the algorithm will show robustness to point clouds with severe missing points (Figure 3). However, more running time will be taken when a large λ is used because a large λ reduces the descent speed of ϵ (Figure 4).

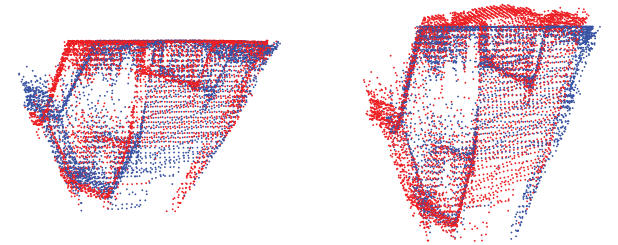
The parameter β_2 plays the role of controlling the maximum mass, which can be transformed between point clouds. The transformed mass reflects the correspondence between two point clouds. The more the mass is transformed between two point clouds, the higher ratio overlap there exists between the two point clouds. When one or two of two point clouds are with severe outliers or missing points, the part of one point clouds can only be accurately matched with other point clouds. In this case, we can adjust the parameter β_2 to improve the accuracy of the registration result. $\alpha_2 = 0$ and $\beta_2 = 1$ means that the ratio of overlap between two point clouds is permitted to be from 0% to 100%. When $0 < \beta_2 < 1$, it means that the ratio of overlap between two point clouds cannot be more than β_2 in our algorithm. In essence, we use β_2 as a prior value of the ratio of overlap between two point clouds. Figure 2 shows the registration results with different β_2 and λ . When the missing ratio between two point clouds is 45%, the accurate registration result can be obtained by setting $\beta_2 = 1$ in Figure 2a. However, a large enough $\lambda = 0.99$ is needed. When the missing ratio between two point clouds is 50% (Figure 3c and 5c), an accurate registration result cannot be obtained by setting $\beta_2 = 1$ and $\lambda = 0.93$. However, when we set $\beta_2 = 0.6$, an accurate registration result can be obtained even if $\lambda = 0.93$. It means that it is easier to obtain an accurate registration result if the

Table 3: Performance on different methods.

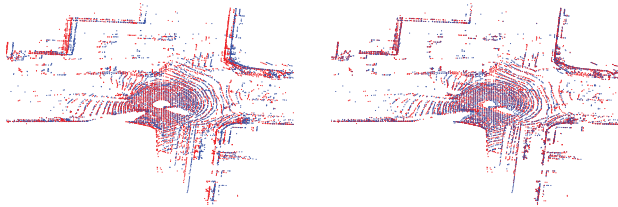
Fig.	10a				10b		11a		11b	
Method	KL	CPD	Ours	KL	CPD	Ours	SPOT	Ours	SPOT	Ours
Angular error	1.614	6.84E-12	3.08E-15	9.24E-13	Failed	4.98E-13	0.088	1.49E-07	0.7980	4.05E-14
Translation error	0.0356	4.76E-6,	6.40E-17	0.036	0.0362	0.0095	0.0844	4.08E-09	0.0607	1.54E-14

Table 4: Performance on real-world data.

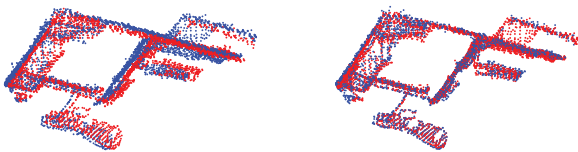
Fig.	Method	Angular error		Translation error	
		mean	max	mean	max
14b	CPD	0.2760	6.4814	2.1981	6.0674
	Trimmed ICP	0.4288	9.2600	2.0454	5.8278
	Ours	0.3277	6.3417	1.8387	7.8279
14c	CPD	1.2194	18.52	0.0376	0.7035
	Trimmed ICP	3.1920	16.6189	0.0438	0.5916
	Ours	1.1908	4.9725	0.0373	0.5990



(a) Lounge data



(b) Apoll SouthBay data



(c) Office Data

Figure 14: Experiments on real-world data.

value of β_2 is set as closer to the ratio of overlap between two point clouds. In the condition that the missing ratio of single point clouds is 55%, the accurate registration result can still be obtained by setting $\beta_2 = 0.6$ (Figure 2b). In Table 2, we demonstrate the role of the parameter β_2 . When the missing ratio of P is 50% in Figure 5, the accurate registration result can be obtained only when $\lambda \geq 0.99$ if setting $\beta_2 = 1$, the accurate registration result can be obtained when $\lambda \geq 0.93$ if setting $\beta_2 = 0.6$. It presents that it is easier to obtain an accurate registration result if the value of β_2 is set as closer to the ratio of overlap between two point clouds. In all experiments, we found that the accurate registration results can be obtained by setting $\beta_2 = 0.6$, even when the overlap ratio is only 30% (Figure 6).

4.2. Robustness and accuracy test on synthetic data

The proposed method is evaluated in this section by comparing it with CPD [MS10], which is the most robust Gaussian-mixture-mode-based algorithm, and Trimmed-ICP [CSK05], which is one of the most popular ICP variants. Two point sets, Bunny model and Dinosaur model, are used. The initial rotation discrepancy between two point clouds P and Q is 50° .

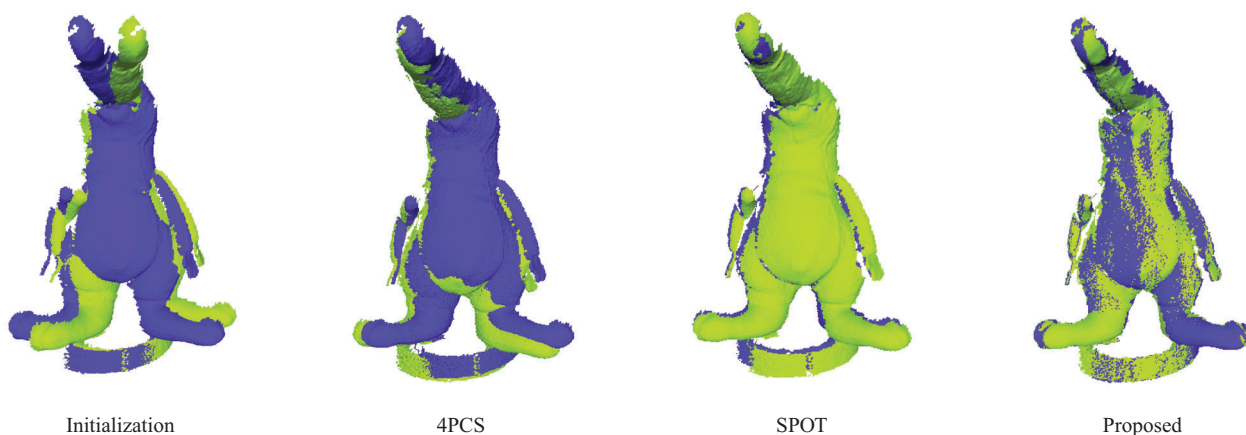
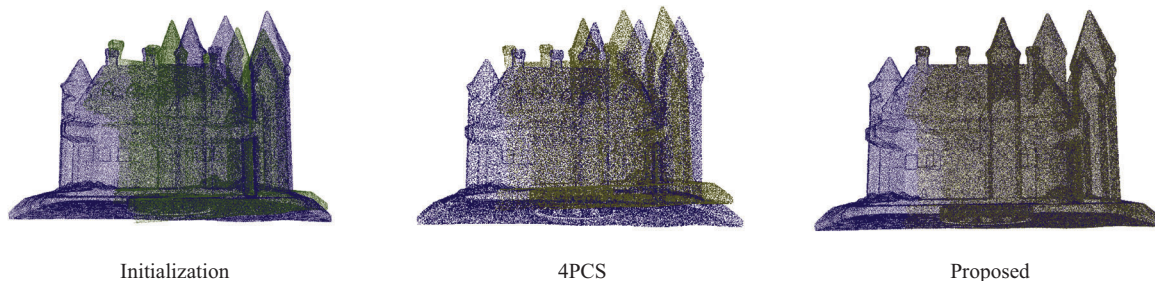
For all experiment results, We make 30 independent runs for all experiment results to obtain the averaged value for comparison. We also make as many experiments as possible for CPD and Trimmed-ICP to find the proper parameters in the two algorithms. The crucial parameters are outlier ratio ω in CPD and closest source points percentage k in Trimmed-ICP.

Point cloud with noise. Figure 7 shows the registration results on point clouds corrupted by a zero-mean Gaussian noise. The optimal transport problem is very robust to noise. Thus, the robustness to noise in our approach and CPD algorithm are shown even when $\sigma^2 = 0.1$ in both case of noise. When $\sigma^2 \geq 0.01$, the accurate results cannot be obtained by trimmed-ICP in both cases of noise.

Point cloud with outlier. The outliers are generated randomly from a zero-mean normal distribution. For Bunny and Dinosaur models, σ of normal distribution is set as 1 and 0.5. We add the different levels of outliers to point cloud P or two point clouds P and Q . The level of outliers is from 0.1 to 1. When the outliers ratio is from 0.1 to 0.5, the parameter λ is set as 0.7. When the outliers ratio is from 0.6 to 1.0, the parameter λ is set as 0.8. The comparisons are shown in Figure 8. The proposed method produced the most robust and accurate results in all experiments, particularly when dealing with point clouds with a large ratio of outliers. The main reason is that the transformed mass can be automatically adjusted step by step during iteration. For example, in the experiment (Figure 8a), the total mass, which is finally transformed between two point clouds,

Table 5: Comparison in running times.

Fig.	Noise (N) Outlier (O) Missing (M)	Size	Time (s)			
			Trimmed ICP	CPD	KL	Ours
7a	N 0.06	1889	–	4.847		5.893
8a	O 60%	3022	–	13.925		16.673
9a	M 25%	1416	–	–		21.301
10a	M 55%	850	–	25.445	–	27.831
10b	M 55%	850	–	–	117.211	20.844
7b	N 0.09	6700	0.958	67.381		60.019
8b	O 50%	10050	–	133.254		138.414
9b	M 20%	5360	–	–		63.993
13b		5000	6.9129	91.2		98.3
13c			1.32	28.7		30.2

**Figure 15:** Registration results on Coati.**Figure 16:** Registration results on WitchCastle.

is 0.6251. This value is accurately matched with the ratio of the number of original points and the number of all points with outliers ($100/160 = 0.625$).

Point cloud with missing points. We delete the points from point clouds P , or delete the different part of points from P and Q to simulate point clouds with missing points. λ is set as $\lambda = 0.99$ When the missing ratio of P is larger than 40% or the missing ratios of P and Q are larger than 20%. In other cases, λ is set as $\lambda = 0.9$. The comparisons are shown in Figure 9. The results demonstrate that the

proposed method owns accuracy with strong stability. The accurate registration result can be obtained from the proposed method when the missing ratios of P and Q are larger than 15%. However, the successful registration results cannot be obtained by CPD and trimmed-ICP.

4.3. Comparison with KL and RG

In Figures 5, 4 and Table 2, we compare the registration results and the running time between KL and RG methods. When the missing

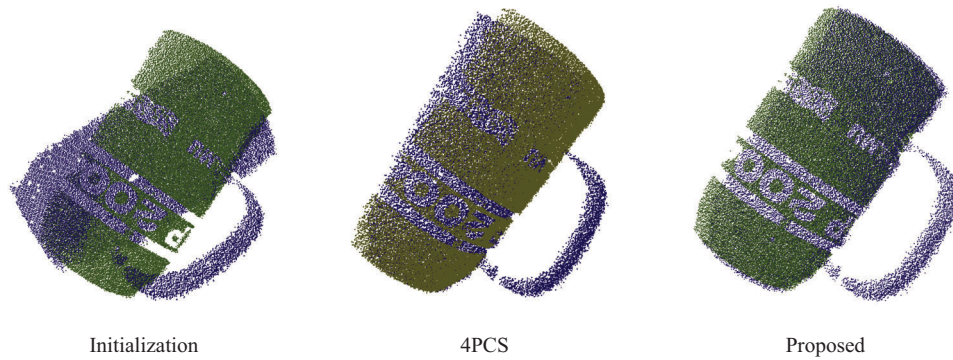


Figure 17: The registration results on Cup.

ratio of P is 50%, as shown in Figure 5, the accurate registration result can be obtained only when $\lambda \geq 0.99$ for KL method, and the accurate registration result can be obtained when $\lambda \geq 0.93$ for RG method. Figure 4 shows that the running time increases with the increase of λ for KL and RG methods. When $\lambda \geq 0.98$, the running time increases exponentially. RG method is more efficient in running time than KL method. In Figure 10, we also compare the registration results on the point clouds with the same missing ratio for KL and RG methods in two experiments with different initial positions (Figures 10a and 10b). Accurate registration results in KL method cannot be certainly obtained when the point clouds have different initial positions. However, the accurate registration results in RG method can be obtained when the point clouds have different missing points. Therefore, RG method is more robust than KL method. The main reason is that KL method is based on a global correspondence, and only partial correspondence is needed in RG method.

4.4. Registration of point clouds with severe missing points

We further demonstrate the robustness of the proposed method by comparing the registration results on point clouds with severe missing points between KL, CPD, SPOT and our approach. In Figure 10, and Table 3, two point clouds with different missing points are aligned with the original point clouds. The proposed method makes the accurate registration results in two challenging examples. However, only one accurate registration result is obtained by KL or CPD methods in the two examples. The experiments show that KL and CPD methods can fall into the local optimal solution when point clouds have severe missing points. The proposed method is more robust than KL and CPD methods. The main reason is that the constraint term of the total mass narrows the solution space. The local optimal solution can be avoided easily in the proposed method.

Figure 11 and Table 3 compares the registration results between SPOT and the proposed approach on point sets with different missing points. Both SPOT and the proposed approach are based on the partial optimal transport. SPOT assumes that all points from the source distributions must be matched to (part of) the target distribution when only one point set has missing points, as shown in Figure 11a. When the part of the source point sets cannot be matched with the target point set in Figure 11b, an accurate registration result cannot be obtained in SPOT. Compared with SPOT, the proposed

approach is only based on the assumption that the overlapped part exists between two point clouds. The proposed method, therefore, obtained the accurate registration results, as shown in Figures 11a and 11b.

4.5. Other model data sets to test robustness

In this section, we applied the proposed algorithm to various point clouds to evaluate the efficiency of our method. In Figure 12, our approach is applied to Bunny models with different missing points. In Figure 13, Bunny model is corrupted by different combinations of noise, outliers and missing points. The experiments show that our method obtains the accurate results even when the point clouds are corrupted by noise, outliers and missing points simultaneously. In Figure 13, considerable data are used to test our method. In Figure 6, aligning two point clouds with only 30% overlap is challenging for traditional ICP methods or soft correspondence method. Our method makes an accurate registration by setting $\beta_2 = 0.6$. The total mass of the final transport plan is 0.2742, which is matched with the overlap of 30%. In Figure 14, the proposed method is applied to Apollo-SouthBay dataset [LZW*19], which is a real-world data. In Figure 14a, only 5000 points, randomly sampled from every original point clouds, are used for registration. In Figure 14b, we first extract one frame data every five frames from original Apollo data set, and 30 frame data is extracted in total. Then, 5000 points, randomly sampled from every frame data, are used for registration. In Figure 14c, we first extract one frame data every three frames from original Office data, and 330 frame data is extracted in total. In Figures 14b and 14c, the registration procedure is that two adjacent frames are matched step by step Table 3. Table 4 shows the performance of different methods on Figures 14b and Fig. 14c. The lowest maximum rotation error and lowest mean translation error have been achieved in our approach. Our approach also makes the lowest mean rotation error in Office data. Trimmed ICP approach has made better performance than our approach in lowest maximum translation error. The main reason is that a global set of parameters have been used for all frame data in our approach. Adapted parameters in our approach need to be considered in the future. For Lounge data, our approach obtains an acceptable registration result from a subjective view. The running times are shown in Table 5. Compared with that in trimmed ICP method, the running time in the proposed method is very long

because of the huge computation cost for the transport plan. This concern is currently a limitation of the proposed method.

In Figure 15, we compare the registration results of 4PCS, SPOT and the proposed method on Coati. In Figures 16 and 17, we further compared the registration results of 4PCS and the proposed method on WitchCastle and Cup. We try our best to obtain many registration results in 4PCS and SPOT on different parameters and same point clouds. The results of 4PCS and SPOT in Figures 15–17 are the most accurate among the results. We can learn from Figures 15 to 17 that the registration results in the proposed methods are more accurate than the registration results in 4PCS and SPOT.

5. Conclusion

We apply the partial optimal transport, a general probabilistic method, to point cloud registration with severe noise, outliers, and missing points. The proposed approach is based on the main finding that some methods, such as CPD and KL, on global correspondences easily fall into the local optimal solution for point clouds registration with severe outliers and missing points. The main contribution of our method is that a range constraint term for total mass is applied in the unbalanced optimal transport. The range constraint term provides an efficient strategy to narrow the solution space. Experiments show that the proposed algorithm performs well on point cloud registration, particularly when point clouds have severe outliers and missing points. We also find that our algorithm has some limitations. The probability measure is based on the assumption that point clouds have a uniform sampling in our algorithm. We will extend our algorithm to the registration of point clouds with high general distribution. Furthermore, we will also improve the time complexity and the adaptivity of the parameters β_2 and λ .

Acknowledgements

The authors wish to thank the anonymous reviewers for their remarks that helped us improving the paper. This work is supported by the grants of Natural Science Foundation of China (61772097).

References

- [AMCO08] AIGER D., MITRA N. J., COHEN-OR D.: 4-points congruent sets for robust surface registration. *ACM Transactions on Graphics* 27, 3 (2008), 1–10.
- [APBC18] ÁLVARO PARRA BUSTOS, CHIN T. J.: Guaranteed outlier removal for point cloud registration with correspondences. *IEEE Transaction on Pattern Recognition and Machine Analysis* 40, 12 (2018), 2868–2882.
- [BC19] BONNEEL N., COEURJOLLY D.: Spot: Sliced partial optimal transport. *ACM Transactions on Graphics (SIGGRAPH)* 38, 4 (2019), 1–13.
- [BM92] BESL P. J., MCKAY N. D.: Method for registration of 3-D shapes. In *Sensor Fusion IV: Control Paradigms and Data Structures*. International Society for Optics and Photonics (Bellingham, Washington USA, 1992), vol. 1611, pp. 586–606.
- [BTP13] BOUAZIZ S., TAGLIASACCHI A., PAULY M.: Sparse iterative closest point. In *Proceedings of the Eleventh Eurographics/ACMSIGGRAPH Symposium on Geometry Processing* (Goslar, DEU, 2013), Eurographics Association, pp. 113–123.
- [CPSV16] CHIZAT L., PEYRÉ G., SCHMITZER B., VIALARD F. X.: Scaling algorithms for unbalanced transport problems. *Mathematics of Computation* 87 (July 2016). <http://doi.org/10.1090/mcom/3303>.
- [CPSV17] CHIZAT L., PEYRE G., SCHMITZER B., VIALARD F.: Scaling algorithms for unbalanced optimal transport problems. *Mathematics of Computation* 87, 314 (2017), 2563–2609.
- [CSK05] CHETVERIKOV D., STEPANOV D., KRSEK P.: *Robust Euclidean Alignment of 3D Point Sets: The Trimmed Iterative Closest Point Algorithm* Alpharetta, GA, USA, (vol. 23), Elsevier, pp. 299–309.
- [EKK18] ECKART B., KIM K., KAUTZ J.: HGMR: Hierarchical gaussian mixtures for adaptive 3D registration. In *Proceedings of the European Conference on Computer Vision (ECCV)* (Cham, 2018), pp. 705–721.
- [FB87] FISCHLER M. A., BOLLES R. C.: Random sample consensus: A paradigm for model fitting with applications to image analysis and automated cartography. In *Readings in Computer Vision: Issues, Problems, Principles, and Paradigms*. Morgan Kaufmann Publishers Inc., San Francisco, CA, USA (1987), pp. 726–740. <http://dl.acm.org/citation.cfm?id=33517.33575>.
- [FCVP17] FEYDY J., CHARLIER B., VIALARD F. X., PEYRÉ G.: Optimal transport for diffeomorphic registration. In *Medical Image Computing and Computer Assisted Intervention*. M. Descoteaux, L. Maier-Hein, A. Franz, P. Jannin, D. L. Collins and S. Duchesne (Eds.). Springer International Publishing, Cham (2017), pp. 291–299.
- [Fit03] FITZGIBBON A. W.: Robust registration of 2D and 3D point sets. *Image and Vision Computing* 21, 13-14 (2003), 1145–1153.
- [FMS19] FROGNER C., MIRZAZADEH F., SOLOMON J.: Learning embeddings into entropic wasserstein spaces. In *Proceedings of the International Conference on Learning Representations* (New Orleans, 2019).
- [FRTG19] FEYDY J., ROUSSILLON P., TROUVE A., GORI P.: Fast and scalable optimal transport for brain tractograms. In *Medical Image Computing and Computer Assisted Intervention*, Springer International Publishing, Cham (2019), pp. 636–644.
- [GMGP05] GELFAND N., MITRA N. J., GUIBAS L. J., POTTMANN H.: Robust global registration. In *SGP'05: Proceedings of the Third Eurographics Symposium on Geometry Processing* (Aire-la-Ville, Switzerland, 2005), Eurographics Association. <http://dl.acm.org/citation.cfm?id=1281920.1281953>.

- [GP02] GRANGER S., PENNEC X.: Multi-scale EM-ICP: A fast and robust approach for surface registration. In *Proceedings of the European Conference on Computer Vision* (Copenhagen, 2002), Springer, pp. 418–432.
- [GT19] GAO W., TEDRAKE R.: Filterreg: Robust and efficient probabilistic point-set registration using gaussian filter and twist parameterization. In *Proceedings of the IEEE Conference on Computer Vision and Pattern Recognition* (Long Beach, 2019), IEEE Computer Society, pp. 11095–11104.
- [HA03] HAILE C., ANAND R.: A new point matching algorithm for non-rigid registration. *Computer Vision and Image Understanding* 89, 3 (2003), 114–141.
- [HZTA04] HAKER S., ZHU L., TANNENBAUM A., ANGENENT S.: Optimal mass transport for registration and warping. *International Journal of Computer Vision* 60, 3 (Dec. 2004), 225–240.
- [JV10] JIAN B., VEMURI B. C.: Robust point set registration using Gaussian mixture models. *IEEE Transactions on Pattern Analysis and Machine Intelligence* 33, 8 (2010), 1633–1645.
- [LWZ*19] LU W., WAN G., ZHOU Y., FU X., YUAN P., SONG S.: DeepVCP: An end-to-end deep neural network for point cloud registration. In *Proceedings of the 2019 IEEE/CVF International Conference on Computer Vision (ICCV)* (Seoul, Korea (South), 2019), IEEE, pp. 12–21. <http://doi.org/10.1109/ICCV.2019.00010>.
- [LZW*19] LU W., ZHOU Y., WAN G., HOU S., SONG S.: L3-Net: Towards learning based lidar localization for autonomous driving. In *Proceedings of the 2019 IEEE/CVF Conference on Computer Vision and Pattern Recognition (CVPR)* (Long Beach, CA, USA, 2019), pp. 6382–6391. <http://doi.org/10.1109/CVPR.2019.00655>
- [MAM14] MELLADO N., AIGER D., MITRA N. J.: Super 4PCS fast global pointcloud registration via smart indexing. *Computer Graphics Forum* 33, 5 (2014), 205–215.
- [MAP15] MAVRIDIS P., ANDREADIS A., PAPAIOANNOU G.: Efficient sparse ICP. *Computer Aided Geometric Design* 35 (2015), 16–26.
- [MS10] MYRONENKO A., SONG X.: Point set registration: Coherent point drift. *IEEE Transactions on Pattern Analysis and Machine Intelligence* 32, 12 (2010), 2262–2275.
- [QCHC17] QIN H., CHEN Y., HE J., CHEN B.: Wasserstein blue noise sampling. *ACM Transactions on Graphics (TOG)* 36, 5 (2017), 168:1–168:13.
- [QHL*19] QIN H., HAN J., LI N., HUANG H., CHEN B.: Mass-driven topology-aware curve skeleton extraction from incomplete point clouds. *IEEE Transactions on Visualization and Computer Graphics* (2019), 1. <http://doi.org/10.1109/TVCG.2019.2903805>
- [RH17] RONGJIE L., HONGKAI Z.: Multi-scale non-rigid point cloud registration using robust sliced-Wasserstein distance via Laplace–Beltrami eigenmap. *SIAM Journal on Imaging Sciences* 10, 2 (2017), 449–483.
- [RTG00] RUBNER Y., TOMASI C., GUIBAS L. J.: The earth mover’s distance as a metric for image retrieval. *International Journal of Computer Vision* 40, 2 (Nov. 2000), 99–121.
- [SDGP*15] SOLOMON J., DE GOES F., PEYRÉ G., CUTURI M., BUTSCHER A., NGUYEN A., DU T., GUIBAS L.: Convolutional Wasserstein distances: Efficient optimal transportation on geometric domains. *ACM Transactions on Graphics (TOG)* 34, 4 (2015), 66:1–66:11.
- [SNB*12] SOLOMON J., NGUYEN A., BUTSCHER A., BENCHEN M., GUIBAS L. J.: Soft maps between surfaces. *Computer Graphics Forum* 31, 5 (2012), 1617–1626.
- [SWS*15] SU Z., WANG Y., SHI R., ZENG W., SUN J., LUO F., GU X.: Optimal mass transport for shape matching and comparison. *IEEE Transactions on Pattern Analysis and Machine Intelligence* 37, 11 (Nov. 2015), 2246–2259.
- [TK04] TSIN Y., KANADE T.: A correlation-based approach to robust point set registration. In *Computer Vision—ECCV 2004*. T. Pajdla and J. Matas (Eds.). Springer Berlin Heidelberg, Berlin, Heidelberg (2004), pp. 558–569.
- [Vil08] VILLANI C.: *Optimal Transport: Old and New* New York, NY, USA, (vol. 338). Springer Science & Business Media, 2008.
- [WS19] WANG Y., SOLOMON J.: Deep closest point: Learning representations for point cloud registration. In *Proceedings of the 2019 IEEE/CVF International Conference on Computer Vision (ICCV)* (Seoul, Korea (South), 2019), SPIE, pp. 3522–3531. <http://doi.org/10.1109/ICCV.2019.00362>
- [YLCJ15] YANG J., LI H., CAMPBELL D., JIA Y.: Go-ICP: A globally optimal solution to 3D ICP point-set registration. *IEEE Transactions on Pattern Analysis and Machine Intelligence* 38, 11 (2015), 2241–2254.
- [ZPK16] ZHOU Q. Y., PARK J., KOLTUN V.: Fast global registration. In *Computer Vision—ECCV 2016*. B. Leibe, J. Matas, N. Sebe and M. Welling (Eds.). Springer International Publishing, Cham (2016), pp. 766–782.